Geophysical Journal International

Geophys. J. Int. (2012) **188,** 421–434 doi: 10.1111/j.1365-246X.2011.05284.x

Earthquakes along Eltanin transform system, SE Pacific Ocean: fault segments characterized by strong and poor seismic coupling and implications for long-term earthquake prediction

Lynn R. Sykes and Göran Ekström

Lamont Doherty Earth Observatory and Department of Earth and Environmental Sciences, Columbia University, Palisades, NY 10964*, USA.*
E-mail: sykes@ldeo.columbia.edu

Accepted 2011 October 25. Received 2011 October 20; in original form 2011 August 16

SUMMARY

Centroid moment tensor solutions are recomputed for 190 earthquakes from 1976 to 2010 along the Heezen, Tharp and Hollister transform faults of the Eltanin system using a 3-D seismic velocity model. The total length of the three *en echelon* faults is nearly 1000 km; each is characterized by fast long-term rates of displacement of about 80 mm yr^{-1}. Strike-slip faulting with moment magnitudes M_w up to 6.4 characterizes most of these events. The few involving normal faulting are located up to 40 km on either side of the transforms and involve extension nearly normal to the transforms. This partitioning of slip likely results from changes during the last few million years in the Euler pole for relative motion between the Antarctic and Pacific plates. Some parts of the Heezen and Tharp transforms exhibit strong seismic coupling but others were aseismic at the resolution of our study, $M_w > 5.0$–5.5. Earthquakes were not found along nearby fast spreading ridges at that resolution. We calculate downdip widths of seismic coupling of about 5 km for four strongly coupled segments from observed moment rates and lengths along strike assuming earthquake activity accounts for the entire plate motion. Major differences in seismic coupling along strike are not in accord with common thermal models of plate cooling but instead are attributed to varying degrees of metamorphism, rock type and effective normal stress and possibly to the presence of short intratransform spreading centres. One 30–42-km-long segment of the Heezen transform that appears to be an isolated well-coupled asperity has ruptured in eight earthquakes of M_w 5.9–6.1 quasi-periodically with a coefficient of variation of 0.26 every 4.0 ± 1.0 yr. Other well-coupled fault segments, which were sites with earthquakes up to M_w 6.39 and fewer events since 1976, have average repeat times of about 7–24 yr. The fast rate of plate motion, maximum size of events and relatively short repeat times make these fault segments a good laboratory for research on quasi-periodic behaviour and earthquake prediction.

Key words: Earthquake interaction, forecasting, and prediction; Seismicity and tectonics; Transform faults; Oceanic transform and fracture zone processes; Dynamics and mechanics of faulting.

1 INTRODUCTION

The ridge segments and transform faults of the East Pacific Rise and Pacific–Antarctic ridge are the sites of the fastest rates of the seafloor spreading and relative plate motion in the world. The Antarctic–Pacific Plate boundary, while characterized by somewhat slower rates than segments of the East Pacific Rise farther north, contains three nearby transform faults—the Heezen, Tharp and Hollister—that together are about 1000 km long and have been the sites of numerous earthquakes of moment magnitude, M_w, 5–6.4 during the past 50 years. They represent a good laboratory for examining fault segments that slip aseismically, others that are well coupled, and the short recurrence times of earthquakes. In this paper we concentrate on these phenomena using earthquakes that have been relocated and reanalysed using long-period digital data from global stations for a recent 35-yr period (Fig. 1).

Recurrence of events along nearly the same fault segment is much more difficult to determine for transform faults on land, such as the San Andreas, where large to great earthquakes typically have repeat times of 100 yr or longer and instrumental data and exact dates for more than one earthquake along a fault segment are rare or non-existent. Palaeoseismically determined dates for earthquakes along

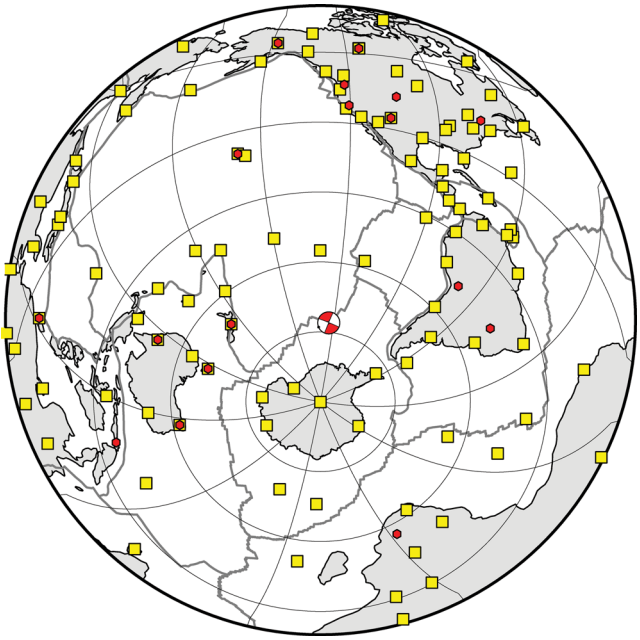

Figure 1. Equidistant polar diagram out to distance of 135 ° centred on our study area, the Eltanin transform system, illustrating distribution of stations that contributed data to CMT solutions. Yellow squares show stations for event of 2007 March 31 of $M_w = 6.2$; the red hexagons show stations for earthquake of 1983 July 5 of $M_w = 6.2$. Strike-slip mechanism in centre is that for 2007 event.

faults of the San Andreas system are uncertain, whereas exact dates are known for the events we examine along the Eltanin transforms. Similarly, earthquake recurrence is more difficult to examine for other long oceanic transform faults, such as those in the equatorial Atlantic, that have considerably smaller long-term slip rates.

2 PREVIOUS STUDIES

In relocating earthquakes along the East Pacific Rise and Pacific–Antarctic Ridge, Sykes (1963) found that the pattern of epicentres was offset about 1000 km near 55 °S. The precision of epicentral locations in his study was improved considerably by using data from new seismic stations in Antarctica that were installed during the International Geophysical Year, 1957–1958, and computer programs for analysing *P* and *PKP* arrival times. Previously, some epicentral locations in that area were uncertain by as much as 500 km. He concluded that a major fracture zone intersected the mid-oceanic ridge at that location, much like those mapped by Menard (1960) farther north. That view was strengthen when Menard reviewed the manuscript and provided an unpublished bathymetric map that included more data in the far southeast Pacific. When Sykes showed his results to M. Ewing, the latter arranged with NSF (US National Science Foundation) for the Research Vessel Eltanin to map the region. The feature was then named the Eltanin fracture zone.

Wilson (1965) utilized the observation that earthquakes along the Eltanin fracture zone were confined to the zone between two offset ridge crests in formulating his hypothesis of transform faulting. Subsequent locations of earthquakes and mapping of bathymetry and magnetic anomalies showed that the Eltanin zone consisted of three *en echelon* transforms (Molnar *et al.* 1975; Lonsdale 1994), which were named for M. Tharp, B. Heezen and C. Hollister (Fig. 2). Aseismic parts of the Heezen and Tharp fracture zones can be traced far to the northwest and southeast. Watts *et al.* (1988) found that at magnetic chron 34, 83–121 Ma, when New Zealand broke away from Antarctica, there was essentially no fault offset at the location where the Eltanin system was later to develop. They found that between chron 27 (61 Ma) and 34 spreading rates were about twice as high to the north of the two transforms than to their south. By chron 28 (63–64 Ma) about 750 km of the present 1000 km offset had accumulated across them. (Ages of chrons are from Gee & Kent 2007). The existence of three or four plates in the region during those times permitted offset to grow across the Eltanin system (Watts *et al.* 1988). The absence of known earthquakes on the three transforms beyond their bounding ridge crests and the spacing of magnetic anomalies, however, indicate that the Pacific and Antarctic plates are intact today beyond the active parts of those transforms and that the lengths of the transforms are not continuing to grow.

Ships have surveyed the active parts of three Eltanin transforms infrequently since they straddle the 'pole of inaccessibility' at the farthest point on the Earth from inhabited land (Lonsdale 1994). They are typified by some of the roughest sea conditions and most severe weather on the Earth. A large iceberg interfered with one scientific mapping (Lonsdale 1994). Only the Heezen transform has been surveyed by swath mapping (Lonsdale 1994). Hence, remote techniques such as seismicity and satellite altimetry provide important constraints on the tectonics, especially for the Tharp and Hollister transforms.

Stewart & Okal (1983) concluded that earthquakes along the Eltanin zone from 1920 to 1981 accounted for less than 10 per cent of the slip predicted by kinematic models of plate motion and cooling. They proposed that the Eltanin transforms consisted of small, well-separated asperities that rupture in earthquakes. Their surface wave magnitudes, M_s, for events before 1969 along the Eltanin system were determined typically from one to a few stations. They also calculated M_w for three earthquakes in 1969, 1971 and 1973; they and Molnar *et al.* (1975) obtained strike-slip mechanisms for them and another event in 1967. Wolfe *et al.* (1993) obtained two normal-faulting mechanisms and computed depths of faulting from waveform matching. Okal & Langenhorst (2000) relocated a number of earthquakes along the three transforms using short-period body waves. Extending the work of Stewart & Okal (1983), they again emphasized the dominance of aseismic slip. They concluded from analyses of seismograms, however, that the transform earthquakes themselves did not have a significant component of slow seismic slip.

Our work using much greater numbers of stations and earthquakes confirms the general findings of Stewart and Okal about the abundance of aseismic slip and the presence of asperities. We show in detail, however, that some segments of the three transforms are aseismic at the $M_w > 5.4$ level whereas others are more strongly coupled. We find that seismic coupling is not merely a function of relative plate velocity, location along the transform and transform length. In studies of transforms along the ultra-fast spreading East Pacific Rise just to the south of the equator, McGuire *et al.* (2005), McGuire (2008) and Boettcher & McGuire (2009) find that some fault segments are characterized by a predominance of aseismic slip while others are fully coupled. Several of those well-coupled segments ruptured quasi-periodically in earthquakes of $M_w \sim 5.5$–6 and with repeat times shorter than 10 yr. We choose the Eltanin transform faults as another good place to search for these phenomena. We find one segment of the Heezen transform has ruptured quasi-periodically since 1976 in eight shocks of M_w 5.9–6.1 with an average repeat time of 4 yr.

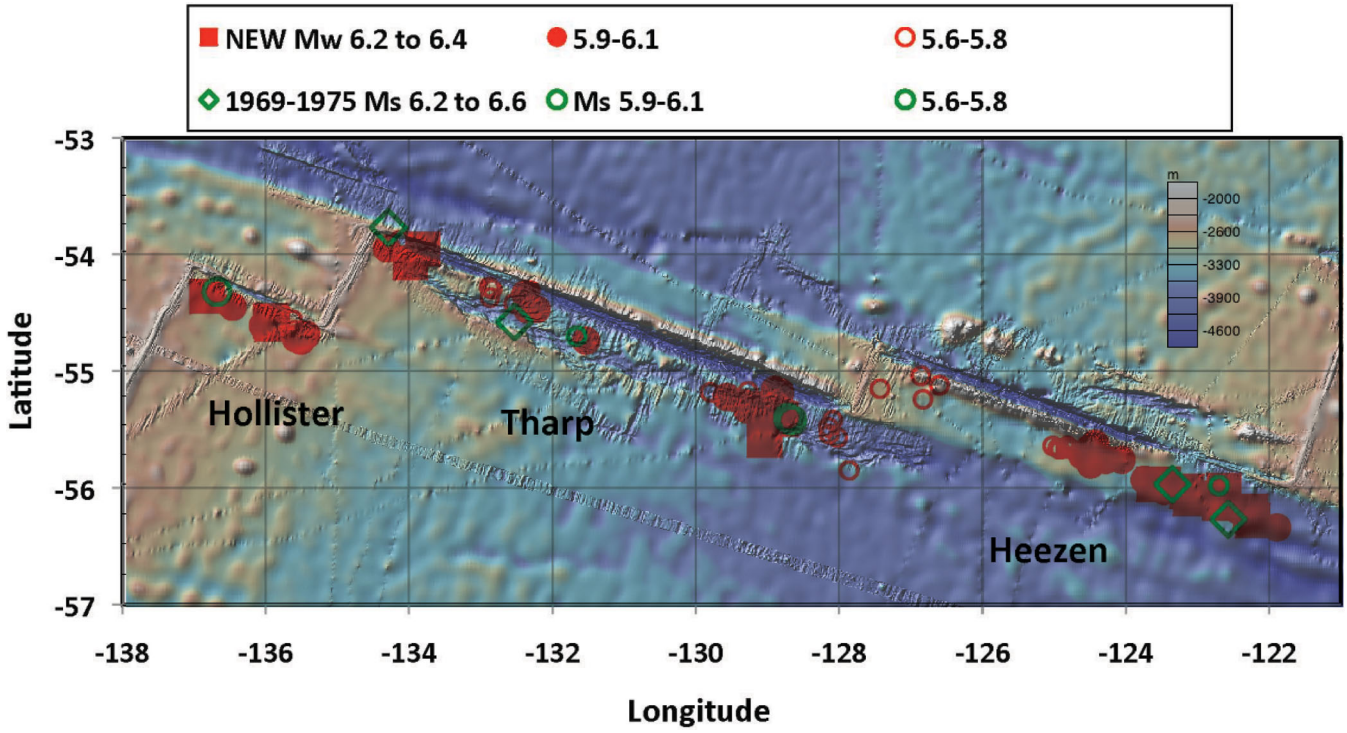

Figure 2. Locations of earthquakes with CMT solutions (red) characterized by a predominance of strike-slip faulting along the Heezen, Tharp and Hollister transform faults of the Eltanin system from 1976 to 2010. New M_w corresponds to seismic moment magnitude recomputed for this study. Nine earthquakes from 1969 to 1975 are shown at their body wave locations of the International Seismological Centre (ISC). Their surface wave magnitudes, M_s, are plotted. Bathymetry from Ryan *et al.* (2009). Most of the earthquakes are mislocated systematically to the south of the three transforms as discussed later. Bar at upper right on map shows water depths in metres.

3 METHODOLOGY

We recomputed centroid moment tensor (CMT) solutions for 190 earthquakes along and close to the three transforms of the Eltanin system from 1976 to 2010. We refer to the magnitudes derived from those moment tensors as either new or recomputed M_ws. Available long-period data for events along the three transforms increased from about 15 to 100 global stations as illustrated in Fig. 1 for events of M_w 6.2 in 1983 and 2007. The greater number of stations in the last 20 years permitted CMT solutions to be obtained for a large number of smaller earthquakes, some as small as M_w 5.15. Except for an event in 1975 we did not reanalyse long-period data for earthquakes prior to 1976, but we utilize the approximate locations of some of those larger events in estimating repeat times.

The earthquakes were analysed using the standard Global CMT (GCMT) algorithm as described in Dziewonski *et al*. (1981), Arvidsson & Ekström (1998) and Ekström *et al.* (2005). In this method, the moment tensor and source centroid are estimated by matching observed long-period three-component seismograms to synthetic waveforms calculated using normal-mode summation. The synthetic waveforms used in the CMT inversion are corrected for lateral heterogeneity using the whole-mantle model of Dziewonski & Woodward (1992) for the body waves and long-period mantle waves, and the phase–velocity maps of Ekström *et al.* (1997) for the intermediate-period, fundamental-mode surface waves. The completeness of the CMT data set as a function of time is described later. We note that our revised catalogue with its additions of more solutions, especially of M_w 5.5–6.0, is more complete than the existing CMT catalogue. The solutions, additional methodology and other pertinent data are described more fully in Appendix A and the Supporting Information.

Since the number and azimuthal distribution of the global long-period stations used in computing the CMT solutions increased dramatically since 1976, especially in the 1990s, we choose to use digital data from as many stations as possible in our analyses rather than from merely the few that recorded most of the events. In contrast, VanDeMark (2006) used few events, a double-difference methodology and a uniform velocity model for Rayleigh waves in calculating revised earthquake locations along the Eltanin transforms. Our calculations for all events have the advantage of having been corrected for lateral heterogeneity with the same model. Surface waves have an advantage for precise locations over body waves since their velocity is much less. They differ in that hypocentres derived using body waves give the location of rupture initiation whereas CMT solutions give centroid locations and origin times.

4 RESULTS

4.1 Distribution of earthquakes along three transforms: well-coupled and poorly coupled fault segments

Fig. 2 shows the areal distribution of strike-slip earthquakes $M_w >$ 5.5 as a function of their recomputed magnitude, M_w, in red along the three transform faults of the Eltanin system. Earthquakes of M_w 6.2–6.4 occur along each transform but larger events are confined to the eastern half of the Heezen, two parts of the Tharp and segments of the Hollister. Since CMT locations are not available before 1976,

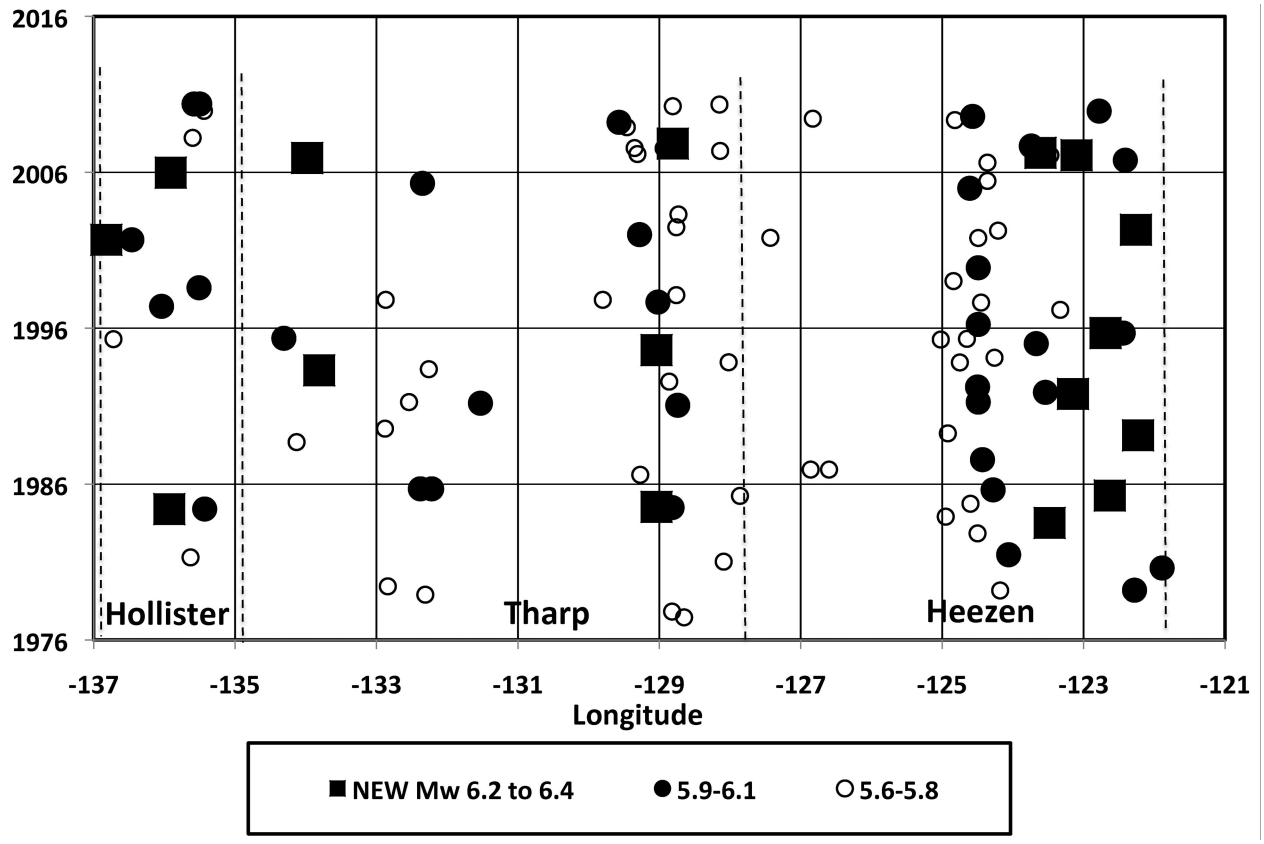

Figure 3. Strike-slip CMT solutions from 1976 to 2010 as a function of longitude along the entire Eltanin transform system. Dotted lines denote approximate locations of ridges.

the 10 largest earthquakes from 1969 to 1975 are shown in green at their body-wave locations of the International Seismological Centre (ISC). All of them occurred along the parts of the transforms that were most active from 1976 to 2010. We take this along with the distributions of events in time and longitude after 1976 (Fig. 3) to indicate stationarity of well-coupled and poorly coupled behaviour along transform segments since at least 1969. The data since 1969 and those of Stewart & Okal (1983) for events back to 1920 indicate that earthquakes of $M_w > 7$ have not ruptured very long segments of any of the transforms.

Figs 4–6 depict the three Eltanin transforms in greater detail. We show events characterized by a predominance of strike-slip faulting that we located since 1976 in red along with the few earthquakes in blue that involved a predominance of normal faulting. No thrust-faulting solutions were found. The axes are each rotated with respect to the Euler rotation pole of DeMets *et al.* (2010) that describes the relative motion of the Pacific and Antarctic plates. The horizontal axis is parallel to computed transform directions; the vertical is perpendicular to it. Distances along the transform are calculated from an arbitrary origin of coordinates at 55.4 °S, 125.0 °W.

Earthquakes of M_w 6.2–6.4 have occurred repeatedly (Fig. 3) along the eastern part of the Heezen transform between +100 and +200 km (Fig. 4). Farther west activity decreases to a maximum of M_w 5.9–6.1 between +30 and +100 km along the fault and then again to a maximum of M_w 5.6–5.8 between +10 and 30 km. A single strike-slip event of M_w 5.15 was obtained along a long section of the western part of the Heezen transform between –110 and +10 km. Clearly, a gradient in the maximum size of earthquakes and seismic coupling occurs between the eastern and western ends of the Heezen transform.

Four segments of the Tharp transform (Fig. 5) are characterized by shocks of $M_w \geq 5.9$ but about half of its length is not. The central part of the Tharp transform near –350 km in Fig. 5 contains only two earthquakes of M_w 5.45 and 5.50. Two 20-km segments of the Hollister transform (Figs 3 and 6) are the sites of several earthquakes of $M_w \geq 5.9$ whereas only single shocks of that size are found along its western half.

4.2 Partitioning of strike-slip and normal-faulting earthquakes in space

Three normal-faulting events were found with *T*-axes nearly perpendicular to the Heezen transform (Fig. 4, between 75 and 125 km). The two largest (M_w 6.7 and 5.9) occurred well to the north of the transform in 2001 and 2007. Wolfe *et al.* (1993) and Lonsdale (1994) concluded that the event of 1984 August 16 (M_w 5.3) was located along a bathymetric trough to the north of the Heezen transform. Hence, it and the two larger events occurred along an off-transform feature. The normal-faulting event of 2001 August 6 is larger than that of any of the strike-slip events along the three Eltanin transforms. Nevertheless, strike-slip earthquakes along the three transform faults are much more numerous and have together released more seismic moment than the normal-faulting events.

Wolfe *et al.* (1993) and Lonsdale (1994) describe three short spreading centres with a total length of about 6 km along the seismically quiet part of the Heezen transform between 125.5 ° and

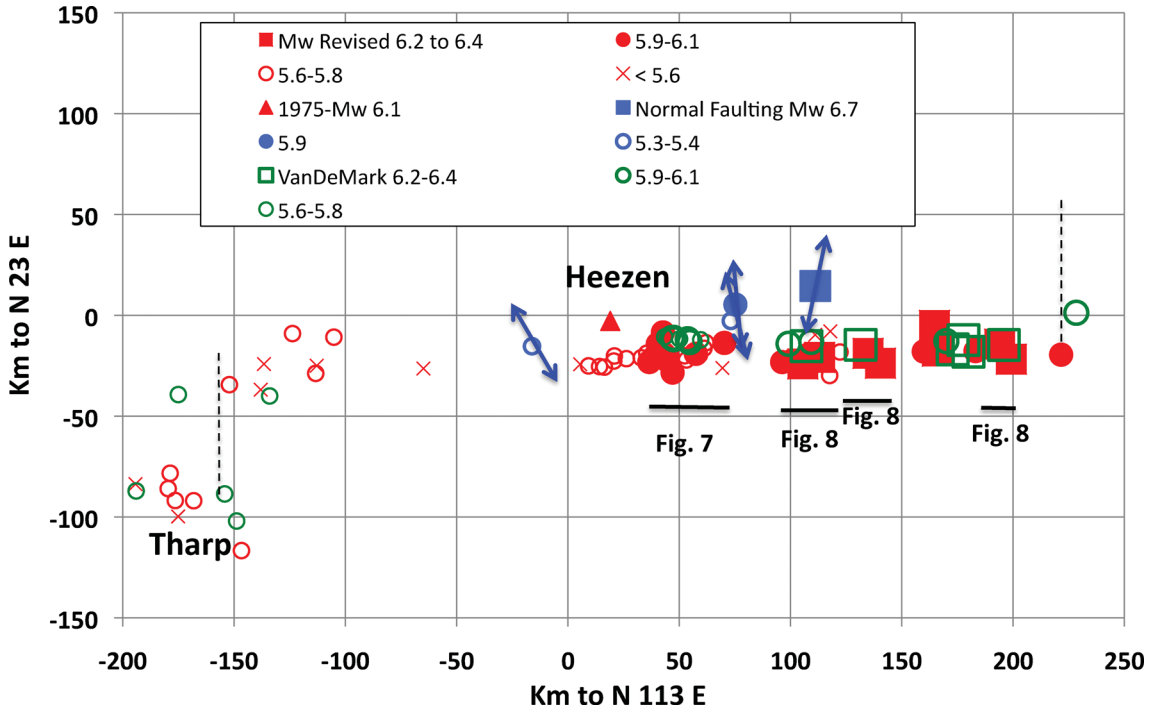

Figure 4. Map view of CMT locations of earthquakes along Heezen transform and easternmost end of Tharp transform from 1976 to 2010. Red and green symbols denote strike-slip faulting. Blue symbols indicate four normal faulting mechanisms and their *T*-(extensional) axes. Red triangle indicates CMT solution for shock of 1975 April 19. Dotted lines denote approximate locations of ridge segments.

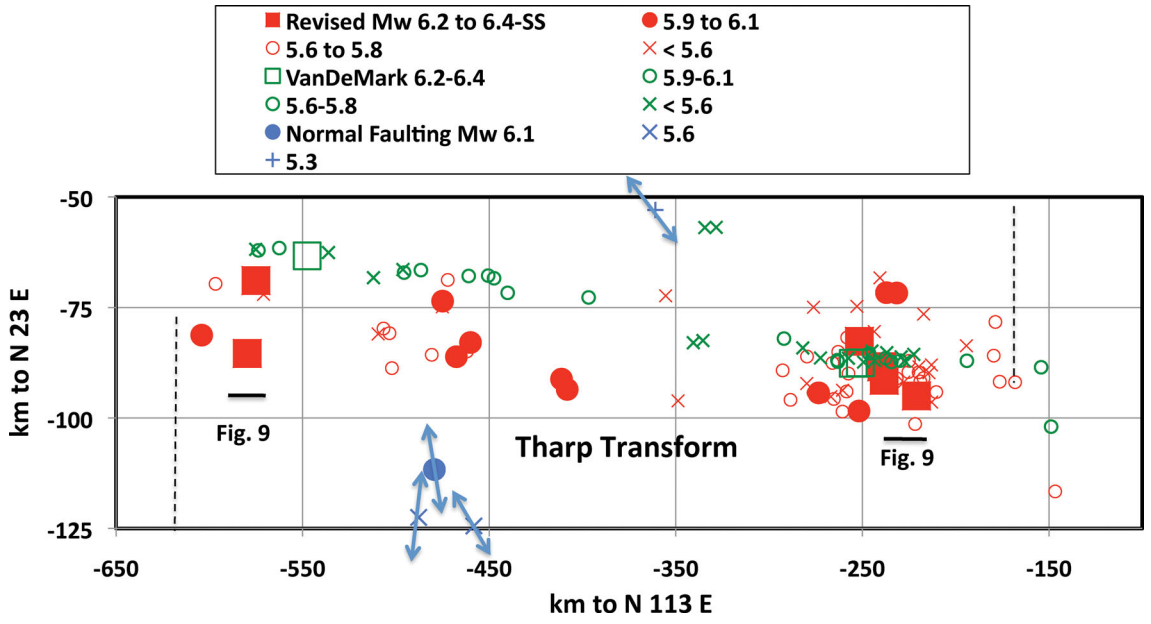

Figure 5. Map view of CMT locations of earthquakes along Tharp transform from 1976 to 2010. Symbols, axes and origin of coordinates same as Fig. 4. Note exaggerated scale in transform-perpendicular direction.

126° W (Fig. 3). The *T*-axis of a normal-faulting event in that area of M_w 5.4 in 1978 is inclined about 45° to the transform (Fig. 4, between –25 km and 0 km). Wolfe *et al.* (1993) attribute it to one of those small spreading centres. If those short spreading centres are very young, they may not have had enough time to become oriented perpendicular to the transform. The relatively small size of that earthquake, its early date and the off-transform locations of other normal-faulting events lead us conclude it more likely occurred just north of the Heezen transform.

Figs 5 and 6 show five other normal-faulting mechanisms adjacent to but not on the Tharp and Hollister transforms. Four of them have *T*-axes nearly perpendicular to those transforms while the smallest of M_w 5.3 in 1982 is oriented about 45° to the Tharp. None of the five is reasonably attributed to a small spreading segment along either of those two transforms. The linearity of the CMT locations along the shorter Hollister transform (Fig. 6) indicates that it may be a single fault. We conclude that strike-slip and normal faulting along the three Eltanin transforms are partitioned so

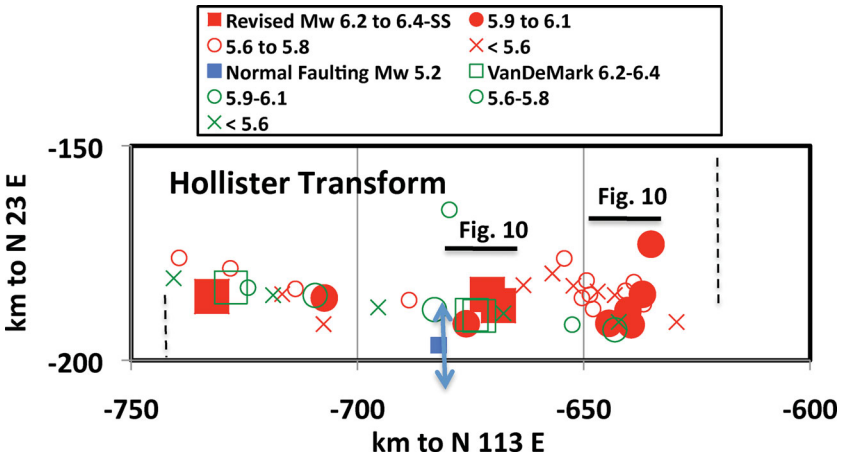

Figure 6. Map view of CMT locations of earthquakes along Hollister transform fault from 1976 to 2010. Symbols, axes and origin of coordinates same as Fig. 4.

that strike-slip faulting takes place along the transforms themselves and normal faulting occurs nearby but just off the transforms.

In detailed swath mapping of three ultra fast-moving transforms just to the south of the equator, Searle (1983) found that each consisted of two or more short transforms bounded by very short spreading centres. He attributed this to changes in the Euler pole for Pacific–Nasca plate motion during the last several million years. Lonsdale (1994) concludes that a zone of extension north of the Heezen transform developed following a Pliocene change in relative plate motion. It is that region where three of the four normal faulting earthquakes in Fig. 4 occurred. Wolfe *et al.* (1993) find that a 10° clockwise rotation of magnetic anomalies north of the Heezen transform occurred within the last 4 Ma, which would put it in extension. Wolfe *et al.* (1993) found another normal faulting event just to the south of the Menard transform fault at 49.5°S along the same plate boundary. They also report reverse faulting events near transform faults at other plate boundaries, another indication of changes in relative plate motion during the last few million years. While off-transform normal-faulting events and short intra-transform spreading centres are reasonably attributed to changes in plate motion, we do not find evidence from earthquake mechanisms along the Eltanin transforms that those faults are 'leaky' today in the sense proposed by Menard & Atwater (1969).

Neither Okal & Langenhorst (2000) nor we found any normal faulting earthquakes along spreading ridges adjacent to the Eltanin fault system. The maximum size of earthquakes along fast spreading ridges themselves is not greater than magnitude 3 (McGuire 2008; M. Tolstoy, personal communication, 2010). Nearby ocean bottom seismometers are needed to detect them. This attests to the very thin lithosphere at fast spreading ridges. In contrast, normal-faulting events of M_w 5–6.5 are common along slower spreading ridges such as those in the Atlantic.

The CMT locations for the Tharp transform are rotated several degrees with respect to both the computed transform direction in Fig. 5 and the bathymetric expression of it in Fig. 2. The sense of the rotation is such that one or more offsets between parts of the Tharp transform would be short compressional features rather than spreading centres. No thrust earthquake mechanisms, however, were found along the Tharp zone. It seems unlikely that our CMT location errors would change much over the length of the Tharp transform. If the anomalous trend is real, having one group of events (east or west) off the primary transform then almost becomes a necessary interpretation. The CMT locations for the Heezen and Hollister transforms and the eastern end of the Tharp are biased to the south of the bathymetric expression of the transforms (Fig. 2). Hence, we suspect that the events at the western end of the Tharp transform are anomalous in some sense.

S. Carbotte (written communication, 2011 July 22) notes, however, that some of the shocks along the eastern end of the Tharp transform might fall within a zone of deformed/rotated seafloor south of the transform that looks quite similar to the zone of deformation north of the Heezen transform described by Lonsdale (1994) and seen in Fig. 2. None of our normal-faulting solutions are found adjacent to that part of the Tharp transform.

4.3 Repeat times of earthquakes along an isolated, well-coupled fault segment

A major purpose of our work is to examine the degree of repeatability (or lack thereof) of major earthquakes along various segments of the three Eltanin transforms. We first examine an unusual case of repeatability of shocks of nearly the same M_w, 6.0. We then examine other segments with fewer but larger earthquakes. We assume that earthquakes along a given segment of a transform occur on single faults although the distribution of CMT solutions scatters about ±15 km perpendicular to the transforms. In detail the distribution of fault segments is likely to be fractal. We postpone a discussion of reasons why various segments were the sites of shocks of differing M_w until the Discussion (Section 5).

A 30- to 42-km segment of the Heezen transform fault between 124.05° and 124.75° W was the site of eight shocks of M_w 5.93–6.07 from 1976 to 2010 (Figs 3 and 4) and possibly an earlier event in 1975. Cumulative moment release along that segment is displayed in Fig. 7 for events of $M_w > 5.55$ (blue) and $M_w > 5.9$ (red). Best-fitting linear relationships are drawn through the dates of earthquakes and the seismic moment that had just been accumulated. Events of $M_w > 5.9$ account for 70 per cent of the moment in Fig. 7. The smaller events in Fig. 7, several of which are aftershocks and foreshocks, are considered to be noise in ascertaining the quasi-periodic behaviour of the larger shocks.

The data for $M_w > 5.9$ are fit remarkably well by the slip predictable model of Shimazaki & Nakata (1980) whereby the size of the next earthquake is proportional to the time since the previous event. The two dotted lines in Fig. 7 are the best fit to that model. The time-predictable model (not shown), in which the time to the next earthquake is proportional to the size of the

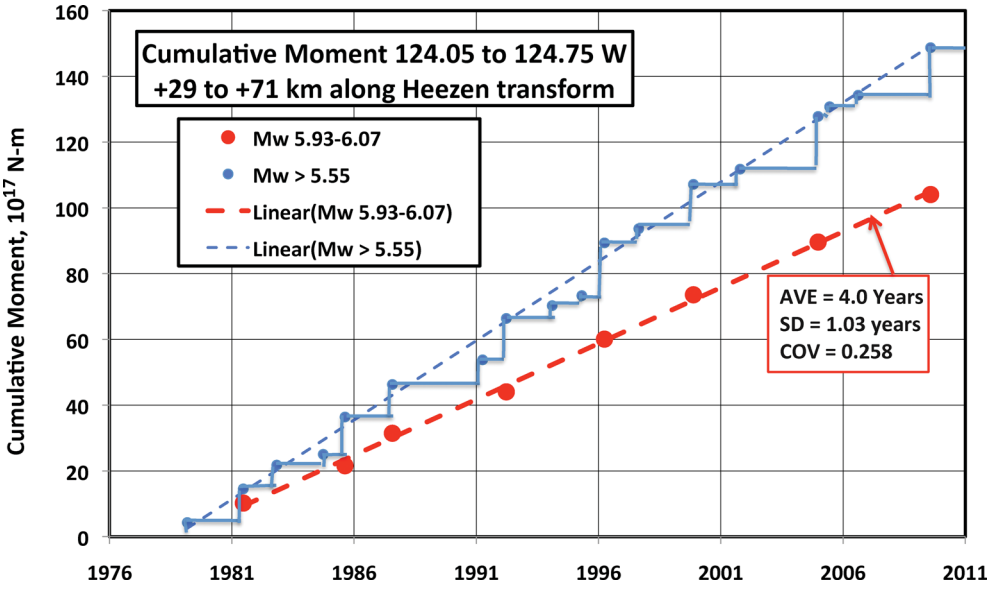

Figure 7. Cumulative seismic moment release from 1976 to 2010 along a 42-km section of Heezen transform indicated in Fig. 4. Distances in kilometres same as in Fig. 4.

preceding large event, also fits the data, though slightly less well. Hence, we cannot distinguish between those two models. The remarkable quasi-repeatability of events of $M_w > 5.9$ may be attributed to the isolation of an asperity, that is, a single resisting fault segment that ruptures mainly or solely in earthquakes. The centroids of events of larger M_w are found at least 35 km eastwards along the Heezen transform and those to its west are relatively small.

The average repeat time for the eight events of $M_w > 5.9$ is 4.0 ± 1.0 (1 *SD*) yr. The coefficient of variation (COV), the standard deviation, *SD*, divided by the average repeat time, is 0.26. Sykes & Menke (2006) calculated maximum-likelihood estimates of COV that were 0.3 or smaller for a number of large-to-great earthquakes that ruptured nearly the same segments of strike-slip and subduction zone faults. COV = 0 and 1.0 correspond to strict periodicity and random occurrence, respectively. McGuire (2008) examined 16 pairs of $M_w \geq 5.5$ earthquakes that occurred along approximately the same segments of transform faults on the East Pacific Rise to the south and north of the equator. He found that interevent times for those pairs was tightly clustered around 5 yr with a COV ~ 0.2. His values and ours of COV = 0.26 imply quasi-periodic behaviour.

The red series in Fig. 7 includes an earthquake on 1981 June 20 of M_w 5.94, which was located just to the east of the others at a time when relatively few stations were available for calculating a CMT location. Excluding it does not change the average repeat time for events of $M_w > 5.9$; it increases the *SD* and COV slightly. Hence, with its inclusion, the series appears to be complete from at least 1981 to 2010. The ISC located an event along the segment of $M_s = 5.5$ on 1975 April 19. That M_s was obtained using a single station. We determined a CMT solution for it using seven digital stations and obtained a M_w of 6.1, a strike-slip mechanism and a location (red triangle) about 20 km west of the group indicated in Fig. 4. Given the uncertainty of its CMT location, we think it is reasonably associated with a previous rupture of the same asperity as in Figs 4 and 7.

McGuire (2008) also found that 1-d aftershock zones extended 30–50 km along strike for $M_w \sim 6$ main shocks for transforms of the East Pacific Rise near the equator. The 2004 Parkfield earthquake of M_w 6.0 had a rupture length of 20–25 km (Johanson *et al.* 2006). The 30- to 42-km length that we used for the repeating events along the Heezen transform in Fig. 7 is not unreasonable for single events of M_w 5.9–6.1. If the 1981 shock were mislocated at least 12 km eastwards, the length of the repeating segment would be about 30 km. The average displacement per earthquake is 0.32 m assuming full coupling and an average repeat time of 4 yr.

4.4 Repeat times of earthquakes along other fault segments

Figs 8–10 show cumulative moment release throughout 2010 for seven additional segments of the three Eltanin faults. Earthquakes of $M_w > 5.55$ were included in each computation. These segments contain fewer events of $M_w > 5.9$ than that in Fig. 7; several were the sites of two or three earthquakes of $M_w > 6.15$. The repeat times of those largest events are longer but uncertain since they are based on few earthquakes.

S. Carbotte (written communication, 2011 July 22) notes that the concentration of earthquakes at the eastern end of the Heezen transform corresponds with the region where the 'inside Corner Rift' of Lonsdale (1994) is found to the north. Lonsdale (1994) states 'My interpretation is that mechanical coupling across the transform valley allows eastward drag by the old thick Antarctic lithosphere to impede the westward movement away from the rise crest of a 20–30-km-wide adjacent strip of thin, newly accreted Pacific lithosphere'.

The segment near the eastern end of the Heezen transform between 179 and 200 km (Fig. 4 and red symbols in Fig. 8) contains six events of $M_w \geq 5.89$ since 1971. Their average repeat time is 7.1 yr and their COV is 0.28. The time intervals again are well fit by the slip predictable model (dotted red line). They may be regarded as quasi-periodic. The series includes two events of 6.17 and 6.18 and one of less certain M_w of 6.5 (Stewart & Okal 1983) on 1971 April 4 that are much larger than the other three. If so, their repeat time was about 16 yr but is based on only three events. That segment may well not be a single isolated an asperity as that in Fig. 7, however,

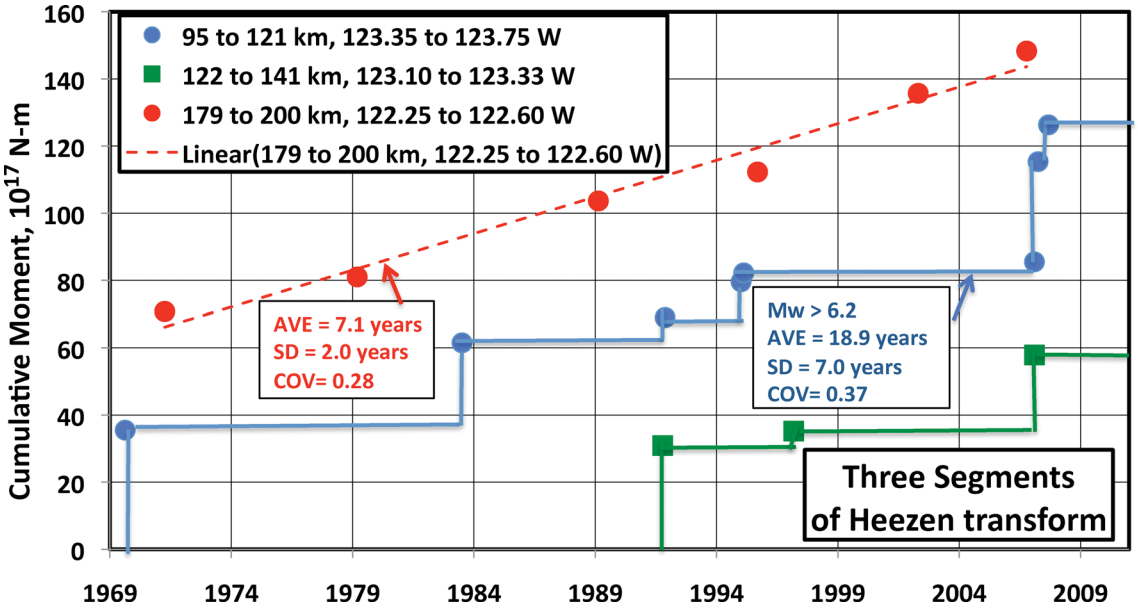

Figure 8. Cumulative seismic moment release for shocks of $M_w > 5.55$ from 1969 to 2010 along three additional segments of Heezen transform fault as indicated in Fig. 4. Distances in kilometres same as in Fig. 4.

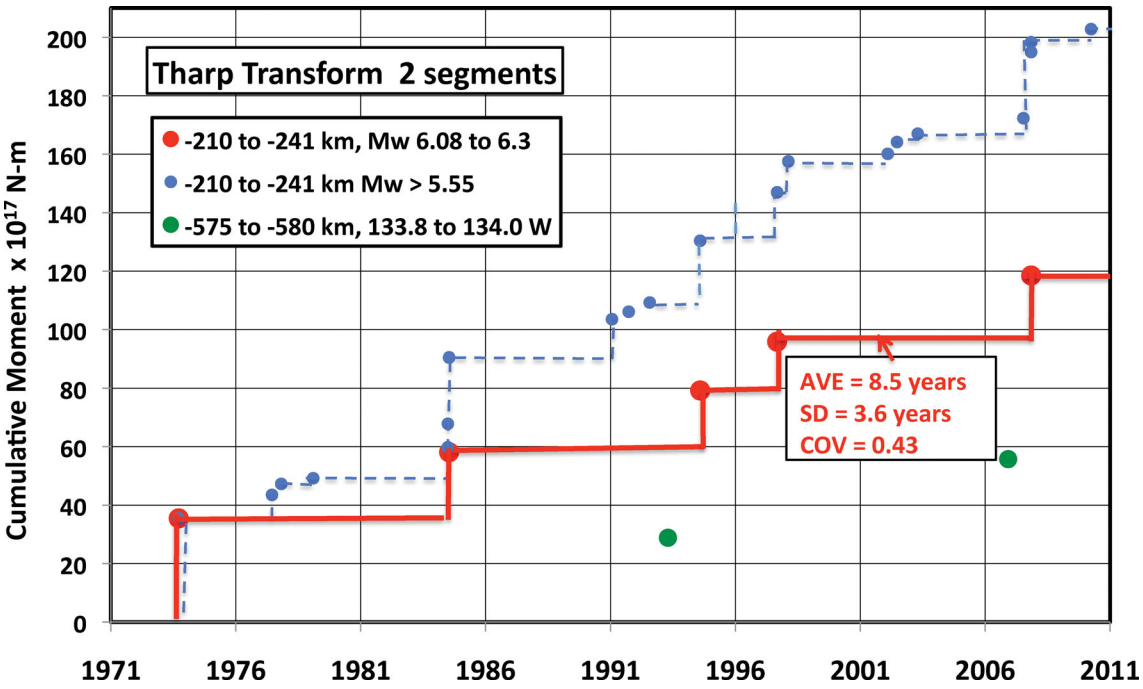

Figure 9. Cumulative seismic moment release 1971 to 2010 along two segments of Tharp transform as indicated in Fig. 5. Distances in kilometres same as in Fig. 4.

since it is located just to the east of other large shocks along the Heezen transform. That may account for the variety of M_ws along it.

Similarly, the series between 95 and 121 km (blue in Fig. 8) includes three events that are much larger than the others in that series. When the event of M_w 6.3 on 1969 August 18 (Stewart & Okal 1983) is included, the repeat time of the three largest shocks is 19 yr with a COV of 0.37. No known large earlier events can be readily attributed to the segment between 122 and 141 km in Fig. 8. Since that segment is adjacent to the one in blue in Fig. 8, interaction between the two may well occur.

Cumulative moment release is shown in Fig. 9 for two sequences of earthquakes along the Tharp transform. The segment between –210 and –241 km consists of a large number of events of $M_w >$ 5.55, one of M_w 6.08, three of $6.15 \leq M_w \leq 6.17$ and one of M_w 6.3 (Stewart & Okal 1983) on 1973 September 18. Moment release in earthquakes of $M_w \geq 6.08$ is about 60 per cent of that for $M_w >$ 5.55. The five largest shocks have a repeat time of about 8 yr and a COV of 0.43. The presence of large events just to its west and the variety of M_ws, however, suggest that it does not always rupture as a single asperity. The segment between –575 and –580 km was the site of only two large earthquakes, M_w 6.22 and 6.24.

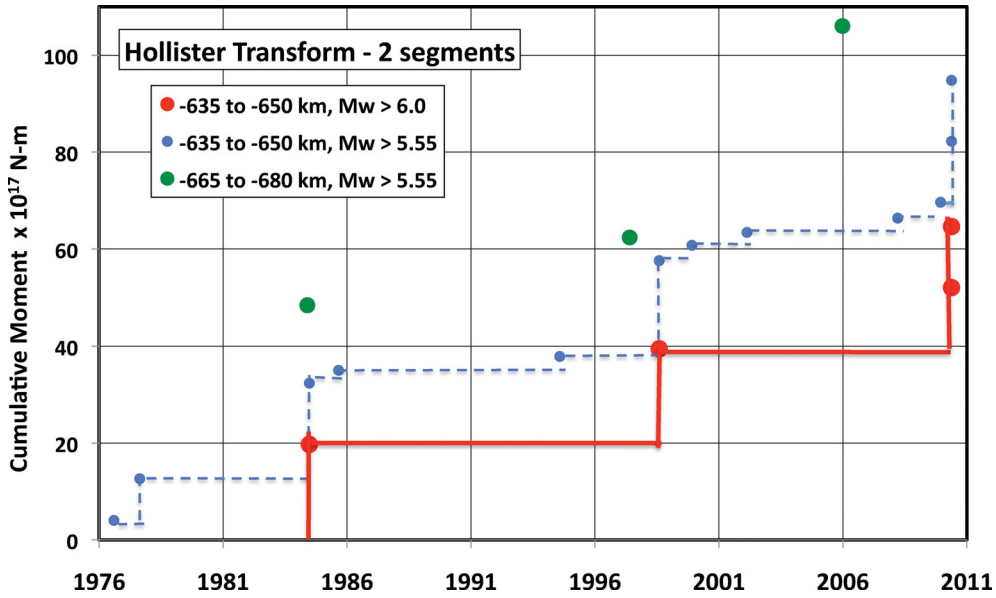

Figure 10. Cumulative seismic moment release for shocks of $M_w > 5.55$ from 1976 to 2010 along two segments of Hollister transform fault as indicated in Fig. 6. Distances in kilometres same as in Fig. 4.

The segment of the Hollister transform between –635 and –650 km (Fig. 10) was the site of many earthquakes of $M_w > 5.55$, two of M_w 6.13 and two of M_w 6.0, the latter two on the same day in 2010. As in Fig. 7, many of the smaller events are either aftershocks or foreshocks and are considered to be noise for the purposes of assessing the repeat times of the largest earthquakes. The three sets of large events have a repeat time of 13 yr and a COV of 0.13. The relationship between the two events that occurred on the same day with computed CMTs only 5 km apart is unknown. It is the only example of a very short time interval between large shocks along segments of the Eltanin transforms.

The fault segment between –665 and –680 km (green symbols in Fig. 10) was the site of events of M_w 6.39, 6.03 and 6.36 in 1984.4, 1997.4 and 2005.98, respectively. ISC located an earthquake along that segment of M_s 6.1 on 1967 September 9. The average of the three intervals since 1967 is 12.8 yr with a COV of 0.36.

For the eight fault segments examined in Figs 7–10 some systematic behaviour can be seen among M_ws of the largest earthquakes, their average repeat times, T, and the numbers of large events. The segment of the Heezen transform between 29 and 71 km (Fig. 7) has the shortest T, 4.0 yr, M_w 5.93–6.07 and eight events. The segment of the Heezen from 179 to 200 km has the next smallest T, 7.1 yr, M_w 5.89–6.5 and six events. The segment of the Tharp transform between –210 and –241 km has a T of 8 yr, M_w 6.08–6.3 and five events. The remaining five segments were the sites of fewer large shocks of M_w 6.0–6.39. Their poorly determined repeat times range from 13 to 24 yr. Hence, a variety of rupture behaviours, repeat times and maximum observed magnitudes is associated with the active parts of the three transforms.

4.5 Calculation of downdip rupture width for several segments of Eltanin Transforms

The CMT centroid depths for events along the Eltanin system are not accurate enough to define the depths or range of seismic faulting at the level of several to 20 km. Computed CMT depths in Table S1 in the Supporting Information range from 12 to 26 km, with 12 being the smallest constrained depth. We instead calculate the downdip width of seismic faulting, W, 'assuming full seismic coupling' for several fault segments, like the ones mentioned above, that have ruptured a number of times in shocks of $M_w > 5.9$ (Figs 4–6). Since the length along strike, L, was not determined for individual earthquakes, for the calculations later we took a length of 105 km for the entire eastern end of the Heezen transform, which includes several segments that have ruptured in large shocks (Fig. 4). We used a 97-km length of the Hollister that includes all large shocks (Fig. 6). Since the 40-km section of the Tharp (Fig. 5) and the 42-km section of the Heezen (Figs 4 and 7) are well isolated from other large shocks along those transforms we took the scatter in locations along them as a measure of L. Our knowledge of L is limited otherwise by the paucity of aftershocks of $M_w > 5$–5.5.

We compute W from the rate of seismic moment release

$$dM_o/dt = \mu L W V_{plate}, \quad (1)$$

where M_o is summed over time periods t, V_{plate} is the rate of relative plate motion and the rigidity modulus $\mu = 2.66 \times 10^{10}$ Pa. In each case we calculated μ for a shear velocity of 3.2 km s^{-1} and a density of 2600 kg m^{-3} for a centroid depth =12 km as in PREM (Preliminary Reference Earth Model of Dziewonski & Anderson 1981). Pacific–Antarctic Plate rates are calculated from DeMets *et al.* (2010).

The four estimates of W in Table 1 range from 3.9 to 6.0 km. The smallest is likely to be an underestimate, since several patches within what we take to be the seismically active part of the Hollister transform were not active at the $M_w \geq 5.9$ level. Somewhat smaller estimates of W are obtained using a value of μ appropriate to the uppermost mantle.

4.6 Calculation of focal depths from body waves

We also analysed the P waves of the two largest normal-faulting events, those of 2001 and 2007 (Fig. 4), to constrain their source depths. The inversion procedure follows the method of Ekström (1989) and leads to estimates of the earthquake focal mechanism, source–time function and point-source depth that are consistent with both the P-wave data and the CMT results. The point source depth

Table 1. Calculation of downdip widths of seismic faulting, W, 1976.0 to 2011.0. The seismically active segments and their lengths are discussed in the text.

Transform segment	Length L (km)	Plate speed v (mm yr^{-1})	Summed moment ΣMo (Nm)	Width W (km)
Heezen[a]	42	79.3	1.49×10^{19}	4.8
Heezen[b]	105	79.3	3.27×10^{19}	4.2
Tharp[c]	40	78.6	1.77×10^{19}	6.0
Hollister[d]	97	77.6	2.72×10^{19}	3.9

[a]For the segment between 124.05° and 124.75°.
[b]For the segment between distance 95 and 200 km in Fig. 4.
[c]For the segment between distance –220 and –260 km in Fig. 5.
[d]For the seismically active portions of transform (Fig. 6).

of 10.4 km places the 2007 earthquake 6–7 km below the ocean floor. For the larger and more complex 2001 earthquake the rupture initiation depth is 8.9 km, and the centroid depth, taking into account the propagation of the point source in the direction of the directivity vector, is approximately 11 km, about 7 km below the ocean floor. The point-source depths are about 10–12 km, which suggests that the earthquakes ruptured faults that cross the M discontinuity. These depths are similar to those determined by Wolfe *et al.* (1993) for two other normal faulting earthquakes off the Eltanin transforms. They obtained a depth in the range 8–14 km below the seafloor for the 1978 earthquake off the Heezen fault, and 'approximately 10 km' below the seafloor for the 1989 earthquake off the Tharp transform.

Whether the depths obtained for normal-faulting events, which occurred off the transforms, applies to strike-slip events along the transforms themselves is equivocal since the velocity and thermal structure of the three transforms is not known and close-in observations with ocean bottom instruments have not been made. Stewart & Okal (1983) modelled P and reflected body waves for several strike-slip events along the Eltanin system. They found that all depths were less than 20 and a few better determined solutions were shallower than 5 km below the seafloor. Nevertheless, modelling body waves is difficult for strike-slip earthquakes along the Eltanin transforms because their amplitudes are small at recording stations that necessarily are at very large distances.

Depths modelled by Wolfe *et al.* (1993) and Abercrombie & Ekström (2001) clearly include the uppermost oceanic mantle for earthquakes along three slower moving transform faults in the Equatorial Atlantic. Since the depth range (Table 1) of faulting in strike-slip events along the Eltanin is very small, those earthquakes may be occurring just in the crust, only in the uppermost oceanic mantle or a combination of the two.

4.7 Completeness of new CMT catalogue and slope of frequency–M_w relationship

The new CMT catalogue that we obtained is more complete than older versions. The efforts that we made, which are described in Appendix A, resulted in a number of additional solutions, especially for the period 1976–1991 and for M_w 5.4–6.0 (see Fig. S1 in the Supporting Information). We obtained a CMT solution for an additional earthquake of M_w 6.15 in 1979. Solutions for new earthquakes of $M_w > 5.5$ were not found after early 2002.

Fig. 11 displays the log of the cumulative number of events per 20 yr as a function of decreasing M_w for the periods 1976–1990 and 1991–2010. The catalogue for the latter period appears to be complete for $M_w > 5.4$–5.5 whereas the earlier period is not complete for $M_w < 6.0$. The slope of –1.0 for the latter period for M_w 5.4–6.0

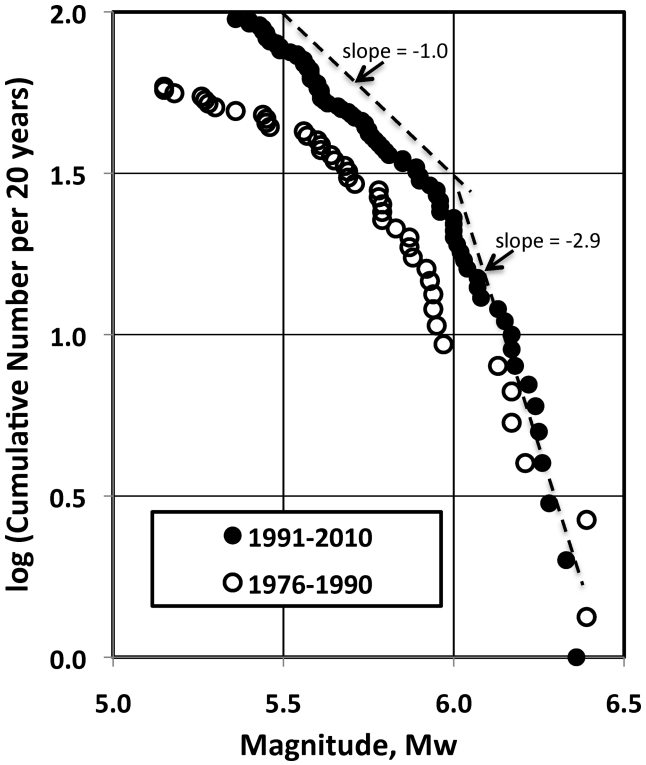

Figure 11. Log of cumulative number of earthquakes per 20 yr larger than a given M_w as a function of M_w. Numbers for 15 yr period 1976–1990 were multiplied by 20/15. Approximate slopes are denoted by dashed lines.

is typical of that for earthquakes in many areas of the world. The steep slope of about –2.9 for $M_w > 6$ is unusual. We interpret it as indicative that only some parts of the three Eltanin transforms are capable of generating shocks of M_w 6.1–6.4 and that events much larger than 6.4, especially events of $M_w > 7$, are unlikely to occur. This is in accord with the findings of Stewart & Okal (1983) that the Eltanin system has not broken in great events since 1920 and is unlikely to do so.

4.8 Precision and accuracy of CMT locations

Table S1 in the Supporting Information lists the formal uncertainties of the revised centroid locations. These are very small, typically 3–15 km for the earliest events and 1–2 km for earthquakes since 2000. These are too small to represent the actual uncertainties. From the scatter of locations perpendicular to the Eltanin transforms, the standard deviation of locations would be around 15 km, after allowing for a constant regional bias. Our locations and those of the ISC based on body waves are located systematically about 25 km south of the transforms as mapped in Fig. 2. This bias suggests that the models used for CMT and ISC locations are not slow enough to the north and northeast along the East Pacific Rise.

VanDeMark (2006) analysed the relative locations of earthquakes of moderate magnitude along oceanic transform faults with a double-difference method using Rayleigh waves of periods between 30 and 80 s. He used 92 events along the Eltanin transform faults from 1980 to early 2006, about half of the number we analysed. His relocations are shown in Figs 4–6 in green. His relocations along the Heezen transform, with one exception, are more tightly clustered than ours. His events along what we identify as a well-coupled zone between 29 and 59 km in Fig. 4 are more tightly clustered in map

view. His results support the idea that events along that segment break a single isolated asperity. We choose to use a greater number of stations as time proceeded rather than use a few common stations as he did. We also used the same 3-D velocity model for our new CMT solutions.

5 DISCUSSION

The combined three Eltanin transform faults are much more active at the $M_w \sim 6$ level than a comparable length of either the San Andreas Fault in California or other transform systems on land. In addition those three oceanic transforms are not as multibranched as many transform zones on continents. Their 1000 km length is greater than that of any other oceanic transforms at fast-spreading plate boundaries. Their length, relative simplicity, 80 mm yr^{-1}, long-term slip rate and the lack of known shocks of $M_w > 7$ make them a good laboratory for studying quasi-periodic recurrence of earthquakes on a timescale of years to a few decades. Their remoteness and rough seas, however, puts a premium on studying them at large distances using seismic waves and various satellite technologies. Knowledge gained from them and other oceanic transform faults may aid in understanding the long-term behaviour of transform faults on land and those at subduction zones where large-to-great earthquakes recur with repeat times of 100 yr or more. Our new catalogue can be used in testing computer simulations of earthquake recurrence.

We find that one isolated asperity along the Heezen transform ruptures about every 4.0 ± 1.0 yr. It and some other segments of the three Eltanin transforms appear to be well coupled seismically. Some other fault segments with larger events rupture with less certain repeat times of 7–24 yr. Other segments are poorly coupled for shocks of $M_w > 5.4$ and perhaps smaller. Our results indicate considerable variation in moment release and hence in fault coupling along the strike of the three Eltanin transforms.

Our findings are in contrast to the widely stated notion that oceanic transform faults, especially those at fast spreading plate boundaries, are poorly coupled with perhaps the presence of occasional stuck patches or asperities. That view comes in large part from assuming that the downdip (vertical) width of seismic faulting extends to about the 600 °C isotherm as calculated using simple conductive plate cooling models where temperature at a given location along the transform is taken as the average on its two sides. In that simple model, earthquakes should extend to greater depths and presumably be larger near the centres of transforms, which is clearly not the case for the Heezen and Tharp faults. Our distributions of earthquakes do not fit other thermal models that we have examined. Some of our largest events occur within about 25 km of the eastern end of the Heezen and the western end of the Hollister transforms (Figs 4 and 6).

Unfortunately, the computed depths of earthquakes along the three Eltanin transforms are not accurate enough to ascertain centroid depths or the downdip width of seismic faulting at the several to 20 km level. Instead, we have chosen not to use models of the depth of seismic faulting in estimating coupling but to calculate downdip width from a segment's length along strike, moment release rate and relative plate rate 'assuming' full seismic coupling. With that assumption we obtain downdip widths of about 5 km for four segments of the Heezen, Tharp and Hollister transforms. Those estimates are smaller than those for oceanic transforms at much slower moving plate boundaries, which is in accord with the notion, which we accept, that temperatures are higher at a given depth for fast moving plate boundaries. If those segments are not fully coupled, our calculations of downdip width, of course, are minimum estimates.

Phipps Morgan & Forsyth (1988), Shen & Forsyth (1992), Behn (2007), Gregg *et al*. (2007) and others modelled temperatures in the vicinity of oceanic transform faults at fast moving plate boundaries that differ from those for the earlier simple plate cooling models. Boettcher & McGuire (2009) conclude that the largest earthquakes on several fast-spreading transforms do not scale directly with the fault area shallower than their calculated 600 °C isotherm. They conclude that the Blanco and Gofar transforms, which were the target of their study, appear to be comprised of multiple patches on a single fault segment that repeatedly fail in earthquakes that rupture each of those patches.

Bohnenstiehl *et al.* (2002) used nearby hydroacoustic stations to locate very small events and aftershocks along a number of oceanic transform faults. They find that aftershock zones of nearby pairs of moderate-size earthquakes along fast-moving transforms were separated by small spreading centres. Lonsdale (1994) mapped a small nearby series of short spreading centres along the Heezen transform, one along the Raitt transform farther north and the Udintsev farther south. Other short spreading centres may exist along the Tharp and other parts of the Heezen transforms. Unless the presence of short spreading centres is taken into account, the application of simple plate cooling models using the entire length of transforms leads to underestimates of temperature and plate coupling.

Finally we are left with what accounts for transform segments that rupture with high seismic coupling and those with low coupling. The presence of short intratransform spreading segments is one factor but others may be differences in hydrothermal alteration and rock type, the sizes of asperities and varying normal stresses and fluid pressures that may place some segments in the velocity strengthening regime and others in the velocity weakening regime. Small amounts of normal faulting occurring off transform is in accord with the idea that the Euler pole has moved relatively recently in time to place each of the three transform zones under a small component of extension. How that may vary along strike and affect seismic coupling is unknown.

For the four seismically active fault segments in Table 1 we obtain similar downdip widths of seismic faulting of about 5 km assuming coupling at the full plate rate. Moment release over 35 yr per unit length along strike for each of those segments is $3.5 \pm 0.7 \times 10^{14}$ N m m^{-1}. These results suggest that asperities responsible for earthquake release at the $M_w > 6$ levels vary in size along strike but not much in downdip width. Nearby asperities, as along the eastern part of the Heezen transform, may break either individually or together. Rupture of two or more nearby asperities in shocks as large as M_w 6.4 can occur but is rare as ascertained from the steep slope of the frequency–magnitude relationship in Fig. 11 for $M_w > 6$. The along strike dimensions and perhaps the downdip widths of asperities must be small for parts of the three Eltanin faults that have not ruptured in events larger than M_w 5.0–5.5. Our knowledge of the Eltanin system is limited by the relatively high magnitude of completeness of events, M_w 5.4, and the paucity of aftershocks and forerunning events.

ACKNOWLEDGMENTS

We thank S. Carbotte and C. Scholz of Lamont and journal reviewers J. McGuire and C. Laederach for critically examining the manuscript and for valuable suggestions and P.G. Richards, W.B.F. Ryan and M. Tolstoy for helpful discussions. S. Carbotte kindly computed the bathymetric map in Fig. 2. GE was partially supported by NSF grant

EAR-09–24694. Lamont-Doherty Earth Observatory Contribution 7505.

REFERENCES

Abercrombie, R.E. & Ekström, G., 2001. Earthquake slip on oceanic transform faults, *Nature,* **410,** 74–77.

Arvidsson, R. & Ekström, G., 1998. Global CMT analysis of moderate earthquakes, Mw ≥ 4:5, using intermediate-period surface waves, *Bull. seism. Soc. Am.,* **88,** 1003–1013.

Behn, M.D., Boettcher, M.S. & Hirth, G., 2007. Thermal structure of oceanic transform faults, *Geology,* **35,** 307–310.

Boettcher, M.S. & McGuire, J.J., 2009. Scaling relations for seismic cycles on mid-ocean ridge transform faults, *Geophys. Res. Lett.,* **36,** L2301, doi:10.1029/2009GL040115.

Bohnenstiehl, D.R., Tolstoy, M., Dziak, R.P., Fox, C.G. & Smith, D.K., 2002. Aftershock sequences in the mid-ocean ridge environment: an analysis using hydroacoustic data, *Tectonophysics,* **354,** 49–70.

DeMets, C., Gordon, R.G. & Argus, D.F., 2010. Geologically current plate motions, *Geophys. J. Int.,* **181,** 1–80.

Dziewonski A.M. & Anderson D.L., 1981. Preliminary Reference Earth Model (PREM), *Phys. Earth planet. Inter.,* **25,** 297–356.

Dziewonski, A.M. & Woodward, R.L., 1992. Acoustic imaging at the planetary scale, in *Acoustical Imaging,* Vol. 19, pp. 785–797, eds Emert, H. & Harjes, H.-P., Plenum Press, New York, NY.

Dziewonski, A.M., Chou, T.A. & Woodhouse, J.H., 1981. Determination of earthquake source parameters from waveform data for studies of global and regional seismicity, *J. geophys. Res.,* **86,** 2825–2852.

Ekström, G., 1989. A very broad band inversion method for the recovery of earthquake source parameters, *Tectonophysics,* **166,** 73–100.

Ekström, G., 2006. Global detection and location of seismic sources using surface waves, *Bull. seism. Soc. Am.,* **96,** 1201–1212.

Ekström, G., Tromp, J. & Larson, E. W. F., 1997. Measurements and global models of surface wave propagation, *J. geophys. Res.,* **102,** 8137–8157.

Ekström, G., Dziewonski, A.M., Maternovskaya, N.N. & Nettles, M., 2005. Global seismicity of 2003: centroid-moment-tensor solutions for 1087 earthquakes, *Phys. Earth planet. Inter.,* **148,** 327–351.

Gee, J.S. & Kent, D.V., 2007. Source of oceanic magnetic anomalies and geomagnetic polarity time scale, *in Treatise on Geophysics,* Vol. 5, pp. 455–507, ed Kono, M., Elsevier, Frankfurt.

Gregg, P.M., Lin, J., Behn, M.D. & Montési, G., 2007. Spreading rate dependence of gravity anomalies along oceanic transform faults, *Nature,* **448,** 183–188.

Johanson, I.A., Fielding, E.J., Rolandone, F. & Burgmann, R., 2006. Coseismic and postseismic slip of the 2004 Parkfield earthquake from space-geodetic data, *Bull. seism. Soc. Am.,* **96,** S269–S282.

Lonsdale, P., 1994. Structural geomorphology of the Eltanin fault system and adjacent transform faults of the Pacific-Antarctic plate boundary, *Mar. geophys. Res.,* **16,** 105–143.

McGuire, J.J., 2008. Seismic cycles and earthquake predictability on east Pacific rise transform faults, *Bull. seism. Soc. Am.,* **98,** 1067–1084.

McGuire, J.J., Boettcher, M.S. & Jordan, T.H., 2005. Foreshock sequences and short-term earthquake predictability on east Pacific rise transform faults, *Nature,* **434**. 457–461.

Menard, H.W., 1960. The east Pacific rise, *Science,* **132,** 1737–1746.

Menard, H.W. & Atwater, T., 1969. Origin of fracture zone topography, *Nature,* **222,** 1037–1040.

Molnar, P., Atwater, T., Mammericks, J. & Smith, S.M., 1975, Magnetic anomalies, bathymetry and the tectonic evolution of the South Pacific since the Late Cretaceous, *Geophys. J. R. astr. Soc.,* **40,** 383–420.

Phipps Morgan, J. & Forsyth, D.W., 1988. Three-dimensional flow and temperature perturbations due to a transform offset, *J. geophys. Res.,* **93,** 2955–2966.

Okal, E.A. & Langenhorst, A.R., 2000. Seismic properties of the Eltanin transform system, South Pacific, *Phys. Earth planet. Inter.,* **119,** 185–208.

Ryan, W.B.F. *et al*. 2009. Global multi-resolution topography synthesis, *Geochem. Geophys. Geosyst.,* **10,** Q03014, doi:10.1029/2008GC002332, 1–9.

Searle, R.C., 1883. Multiple, closely spaced transform faults in fast-slipping fracture zones, *Geology,* **11,** 607–610.

Shen, Y. & Forsyth, D.W., 1992. The effects of temperature and pressure-dependent viscosity on three-dimensional passive flow of the mantle beneath a ridge-transform system, *J. geophys. Res.,* **97,** 19 717–19 728.

Shimazaki, K. & Nakata, T., 1980. Time-predictable recurrence model for large earthquakes, *Geophys. Res. Lett.* **7,** 279–282.

Stewart, L.M. & Okal, E.A., 1983. Seismicity and aseismic slip along the Eltanin fracture zone, *J. geophys. Res.,* **88,** 10 495–10 507.

Sykes, L.R., 1963. Seismicity of the South Pacific Ocean, *J. geophys. Res.,* **68,** 5999–6006.

Sykes, L.R. & Menke, W., 2006. Repeat times of large earthquakes: implications for earthquake mechanics and long-term prediction, *Bull. seism. Soc. Am.,* **96,** 1569–1596.

VanDeMark, T.F., 2006. Moderate and large earthquake activity along oceanic transform faults, *MSc thesis*, Pennsylvania State Univ., 80 pp.

Watts, A.B., Weissel, J.K. & Duncan, R.A., 1988. Origin of the Louisville ridge and its relationship to the Eltanin fracture zone system, *J. geophys. Res.,* **93,** 3051–3077.

Wilson, J.T., 1965. A new class of faults and their bearing on continental drift, *Nature,* **207,** 343–347.

Wolfe, C.J., Bergman, E.A. & Solomon, S.C., 1993. Oceanic transform earthquakes with unusual mechanism or locations: relation to fault geometry and state of stress in the adjacent lithosphere, *J. geophys. Res.,* **98,** 16 187–16 211.

APPENDIX A: DETERMINATION OF CMT SOLUTIONS

Fig. S1 in the Supporting Information shows the revised CMT solutions for 186 earthquakes from 1976 to 2009 on the left and those in the online catalogue on the right. Moment magnitudes are given below each solution. Events in 2010 were determined in the same manner and are listed in the catalogue of the GCMT project at http://www.globalcmt.org. The CMT methodology and format of the catalogue are described in Dziewonski *et al.* (1981) and Ekström *et al.* (2005).

We used a box from 54 °S to 58 °S and 140 °W to 120 °W to identify earthquakes that might be located on the Eltanin transform system. For the period 1976–1989, we selected for analysis all events in the ISC (International Seismological Centre), PDE (Preliminary Determination of Epicentres of the US Geological Survey) and GCMT catalogues, regardless of magnitude. This yielded 84 earthquakes. From 1990 to 2009, we selected events in the ISC, PDE, GCMT and surface wave detection (SWE) catalogues with at least one magnitude equal to or greater than 5.5. We did not use the ISC catalogue for events after 1999. The surface wave catalogue (Ekström 2006) starts in 1990, and the magnitude that is associated with events in that catalogue is usually very close to the M_w obtained in a CMT analysis. It is therefore unlikely that the event selection for 1990–2009 missed any earthquake with a moment magnitude greater than 5.5. This yielded 110 earthquakes for that period. This completeness can be seen as well by the slope of –1.0 of the LogN–M_w relationship in Fig. 11 between M_w 5.4 and 6.0 for events from 1991 to 2010.

Data for the reanalysis were collected from all the main global digital networks that have operated since 1976. This includes the HGLP, SRO and ASRO networks in the 1970s, the SRO, ASRO, DWWSSN, CDSN and Geoscope networks for the 1980s, and the IRIS/USGS GSN, Geoscope, GEOFON and MedNet networks since the 1990s. The waveforms were edited using the standard Global CMT (GCMT) automated waveform editor, and inverted using the standard Global CMT computer codes using corrections for 3-D

earth structure in the calculation of synthetic seismograms (Ekström *et al*. 1997, 2005). Of the 84 earthquakes from 1976 to 1989, we rejected seven CMT solutions. They were generally too small to generate stable CMT results. For the period 1990–2009, we rejected only one event, which occurred on 2001 August 6. This shock of m_b 5.6 in the PDE catalogue occurred only 4 min after the M_w 6.7 normal-faulting event near the Heezen transform, and the waveforms are not sufficiently separated to make a CMT analysis possible.

Intermediate-period surface waves have been used in the GCMT analysis since 2004, and often are very useful for constraining solutions for earthquakes smaller than $M_w = 5.5$. Most of the earlier earthquakes analysed here are larger than $M_w = 5.5$, since smaller earthquakes appear to have gone largely undetected until the 1990s. The new results that include surface wave data are not very different from the earlier results. One exception to this general observation is the earthquake on 2000 October 4. The mechanism in the GCMT catalogue indicates normal faulting, while the reanalysis resulted in a strike-slip mechanism. The new result is well constrained by the surface wave data, which were not included in the original analysis.

APPENDIX B: TRADE-OFF BETWEEN SCALAR–MOMENT ESTIMATES AND DEPTHS OF CMTS

The excitation of the long-period waveforms used in the CMT analysis does not vary rapidly as a function of source depth for shallow-focus earthquakes. This translates into a lack of sensitivity of the CMT algorithm in the estimation of the centroid depth, and instances in which the centroid depth differs appreciably from the true depth of the earthquake, here considered the centre of seismic moment. Experience has shown that deviations of the CMT centroid depth from the true depth occur both randomly and systematically. The random variations can be considered a consequence of the complicated trade-offs that occur when noisy data are fit with synthetic seismograms that do not capture the full complexity of wave propagation in the Earth. Systematic deviations can occur when the Earth structure in the source area deviates significantly from the structure assumed in the calculation of synthetic seismograms, that is, from PREM (Dziewonski & Anderson 1981).

Regardless of the cause of the deviation of the centroid depth from the true depth, the question arises whether an incorrect centroid depth can cause the scalar seismic moment, M_o, estimate to differ from the true moment in a systematic way. For example, if it is known that an earthquake occurred at a depth of 10 km, and the CMT was calculated at 25 km, is there a corresponding bias in the CMT estimate of M_o? Specifically, in the study of the Eltanin earthquakes, we have obtained depths ranging from the shallowest used in the CMT algorithm (12 km) to 26 km. If we assume that all of the true depths of these earthquakes are shallow, what size error or bias should we expect in estimates of M_o?

To address part of this question, we performed the following experiment. We chose one of the Eltanin earthquake of (2009 May 7, $M_w = 5.6$) for which the CMT centroid depth is 25.7 km, and calculated the CMT at various fixed depths, inverting as usual for all the other parameters. The centroid epicentre and time did not shift appreciably in these different inversions, nor did the geometry of the moment tensor change appreciably. We found that M_o evaluated at 10-km depth is 15 per cent smaller than that calculated at the best-fitting centroid depth (25.7 km). This is a much smaller difference than might have been anticipated from ratios of body-wave radiation amplitudes or other methods. Also, there was no discontinuous change in the calculated M_o when the CMT was evaluated above the Moho (which in PREM is at 24.4 km) or below it. This is a consequence of the continuity of displacement eigenfunctions for surface waves across discontinuities, and the dependence of the excitation on these displacements.

This experiment addresses one component of the potential bias that may be present in CMT seismic moments. The experiment suggests that when the CMT depth is larger than the true depth, the estimated Mo is too high by a small amount. For the Eltanin events, this bias is unlikely to be larger than 15 per cent, even for the events with the deepest calculated centroids.

APPENDIX C: COMPARISON OF MAGNITUDES—M_w, M_s and m_b

Our calculations of moment magnitude M_w are compared with determinations of the short-period magnitude m_b in Fig. C1. M_w is systematically higher than m_b for strike-slip events along the three transforms, on average about 0.5 units. This is not surprising since all stations are at large teleseismic distances. Those *P* waves left hypocentres close to the intersection of the two nodal planes (*B*-axis) where their amplitude is very small. Observed *P* waves for a normal-faulting event, however, leave close to their maximum radiation on the focal sphere. We determined a few CMT mechanisms for which PDE or ISC did not compute hypocentres, for which we relied on detections and locations based on intermediate-period surface waves (Ekström 2006). Thus, the use of the CMT methodology insured more complete coverage of earthquakes in this very remote area of the Earth.

Fig. C2 shows that M_w is similar to M_s at larger magnitudes but is 0.4–0.9 units larger at M_w 5.4. Our determinations of M_w

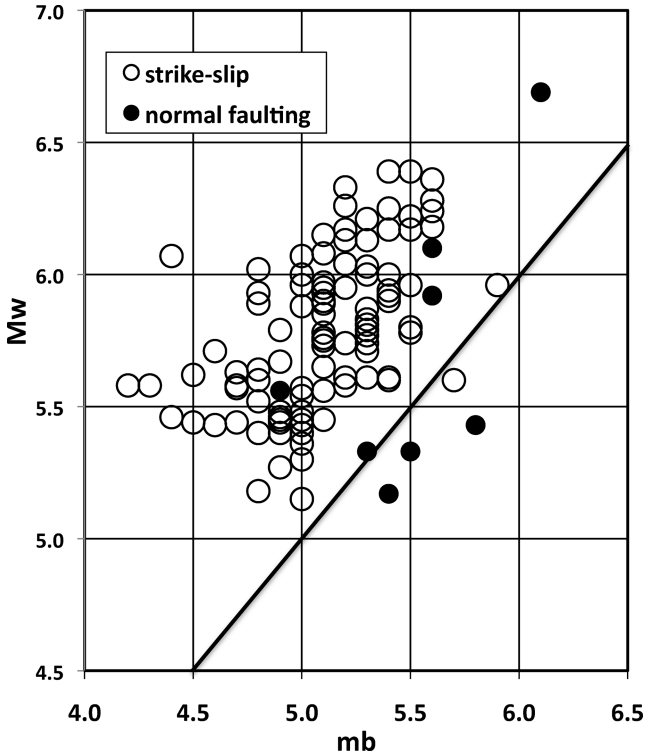

Figure C1. M_w determined in this study compared with short-period body-wave magnitude m_b as computed by either ISC or PDE. Solid line indicates $M_w = m_b$.

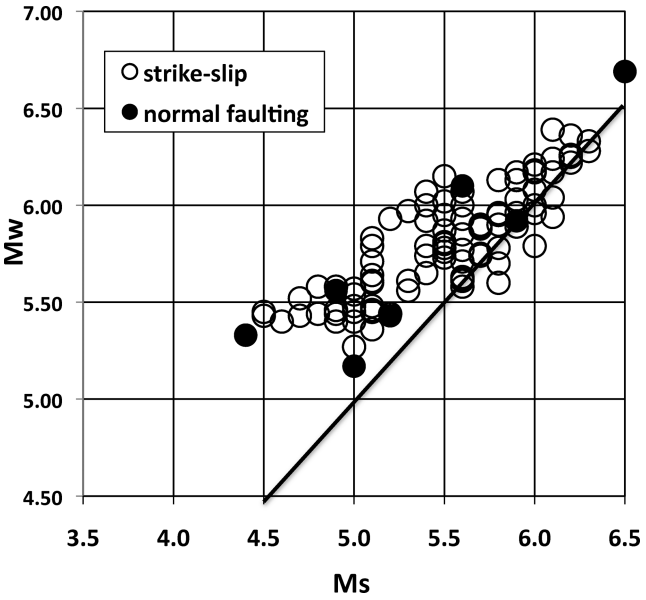

Figure C2. M_w determined in this study compared with the surface wave magnitude M_s as computed by either ISC or PDE for periods between about 17 and 22 s. M_w is determined at longer periods. Solid line indicates $M_w = M_s$.

typically use observations at more stations than those of M_s. Those for M_w also use Love and Rayleigh waves. M_s, which is typically reported by PDE and ISC only for Rayleigh waves and for periods between about 18 and 22 s, may yield a biased estimate of the long-period character of a seismic source as a result of low excitation at certain focal depths and biased sampling of the radiation field. In discriminating the signals of earthquakes from those of underground nuclear explosions low excitation of Rayleigh waves in the narrow period band used for determining M_s may result in a few earthquakes appearing to be explosions. In those circumstances the use of longer period Rayleigh and Love waves, as in the CMT methodology, can lead to those events being identified confidently as earthquakes.

SUPPORTING INFORMATION

Additional Supporting Information may be found in the online version of this article:

Table S1. Centroid moment tensor solutions for 186 earthquakes. Table headings are as in previous CMT reports (Ekström *et al*. 2005). δt_o, $\delta\lambda_o$, $\delta\phi_o$ and δh_o are differences between respective parameters for CMT solutions and hypocentral locations of either ISC or PDE. For a small number of earthquakes, the event time is that determined in our surface wave analysis, since the NEIC did not detect/locate the event.

Figure S1. Revised CMT solutions on left for earthquakes along Eltanin transform system displayed using lower hemisphere, equal-area projections and those in online GCMT catalogue www.globalcmt.org/CMTsearch.html on right. Moment magnitude shown below each solution; dates in years, month, day, hour and minute at top.

Please note: Wiley-Blackwell are not responsible for the content or functionality of any supporting materials supplied by the authors. Any queries (other than missing material) should be directed to the corresponding author for the article.